J. Phys.D: Appl. Phys., 37 2918-2924 (2004), DOI: 10.1088/0022-3727/37/20/021

Study of microscopic properties of water fullerene suspension by means of resonant light scattering analysis

D Jakubczyk, G Derkachov, W Bazhan, E Łusakowska, K Kolwas and M Kolwas

Institute of Physics of the Polish Academy of Sciences, al.Lotników 32/46, 02-668 Warsaw, Poland

E-mail: jakub@ifpan.edu.pl

Abstract. Scattering of coherent light by a droplet of water fullerene suspension was investigated. Two light wavelengths were used simultaneously. The evolution of radius and refractive index of a droplet was examined. Resonant scattering was detected and analyzed by means of a simple model and some conclusions were drawn on the microscopic properties of suspension. The study was supplemented with Atomic Force Microscopy measurements of samples obtained by drying the suspension.

PACS numbers: 42.25.Fx, 42.25.Dd, 68.03.Fg, 61.48.+c, 61.46.+w

Submitted to: *J. Phys. D: Appl. Phys.*

1. Introduction

Suspensions are nearly omnipresent and there are many well established techniques to study them. Let us mention a few of them. First of all there are purely mechanical techniques, such as centrifugation and sieving. Secondly there is microscopy: classical optic (also scanning), near-field optic, electron, atomic force, etc. There are also various scattering techniques: static light scattering, dynamic light scattering, small-angle X-ray or neutron scattering, etc. [1, 2] All these techniques have their scopes of applicability and many of them are not interchangeable. For instance, for such suspensions as encountered in aerosol droplets an *in situ* technique would be strongly preferable, since abandoning the form of a droplet (drying, centrifuging, sieving) would weight heavily upon the measured properties of suspension. On the other hand, out of many properties, the optical properties of aerosol suspensions are especially interesting due to their impact upon the climate on Earth [3]. For example, carbonaceous soot aerosol seems to play important role in the micro physics of clouds. Soot clusters often form agglomerates with water microdroplets which can induce profound changes of droplet optical properties (compare e.g.: [4]). Soot clusters and nanostructured materials has been extensively

investigated for decades (e.g. [5]). The optics of water microdroplets with carbonaceous inclusions was studied e.g. by Chýlek [3] and more recently theoretically by Markel [6, 7], where broad literature of the subject can be found.

2. Experiment

2.1. The outline of the method

Since we've been interested in atmospheric aerosols, we adopted a static light scattering technique. This technique enables to follow the evolution of effective refractive index of the evaporating suspension droplet as well as the radius of the droplet. Due to evaporation the contents of carbon is changing - from very low at the beginning to very high at the moment of the droplet size stabilization (sometimes totally dry object). We have observed that evaporating droplets of suspension exhibit discrepancy of their refractive index as a function of inclusions density from standard effective medium theory prediction. We have extended a simple model of scattering of light by a single microdroplet of simple suspension to water containing fullerene nanocrystallites. By these means we try to infer about the physical properties of the suspension. So far, we have applied our method to two kinds of suspensions. First we used a very simple and well defined (though rather unrealistic): monodispersive water suspensions of SiO_2 and PS (polystyrene) spheres [8]. For this work we have used a more realistic (but still a little exotic) suspension of fullerene nanocrystallites in water. The water suspension of fullerene (nano)crystallites imitates soot particles dispersed in water but is also of interest as such (e.g. medical [9]) and had been investigated [10, 11, 12].

We have supplemented our investigation of fullerene water suspensions with an Atomic Force Microscopy (AFM) (MultiMode SPM, DI) study of samples obtained by drying the suspension, also in order to be able to compare the results with those of other authors.

The diagram of experimental setup is presented in figure 1. An electromagnetic quadrupole trap [13] kept in the small climatic chamber is in its heart [14]. We were able to trap droplets in range of a diameters from a few microns to a few tens of microns.

2.2. Sample preparation and thermodynamic conditions

Fullerene nanocrystallites water suspension was prepared by stirring or sonicating fullerene powder (99% C_{60}, MER) in distilled (in some cases ultrapure) water and filtering through a filtering paper (~ 15 μm pore size) shortly before the experiment. In most cases the samples were also filtered through a 450 nm pore size filter (SM11306, Sartorius). At the stage of preparation we were not able to estimate the concentration of suspension.

The thermodynamic conditions of our experiments: temperature T and relative humidity S in the chamber and atmospheric pressure p_{atm} are given in figure 4 caption.

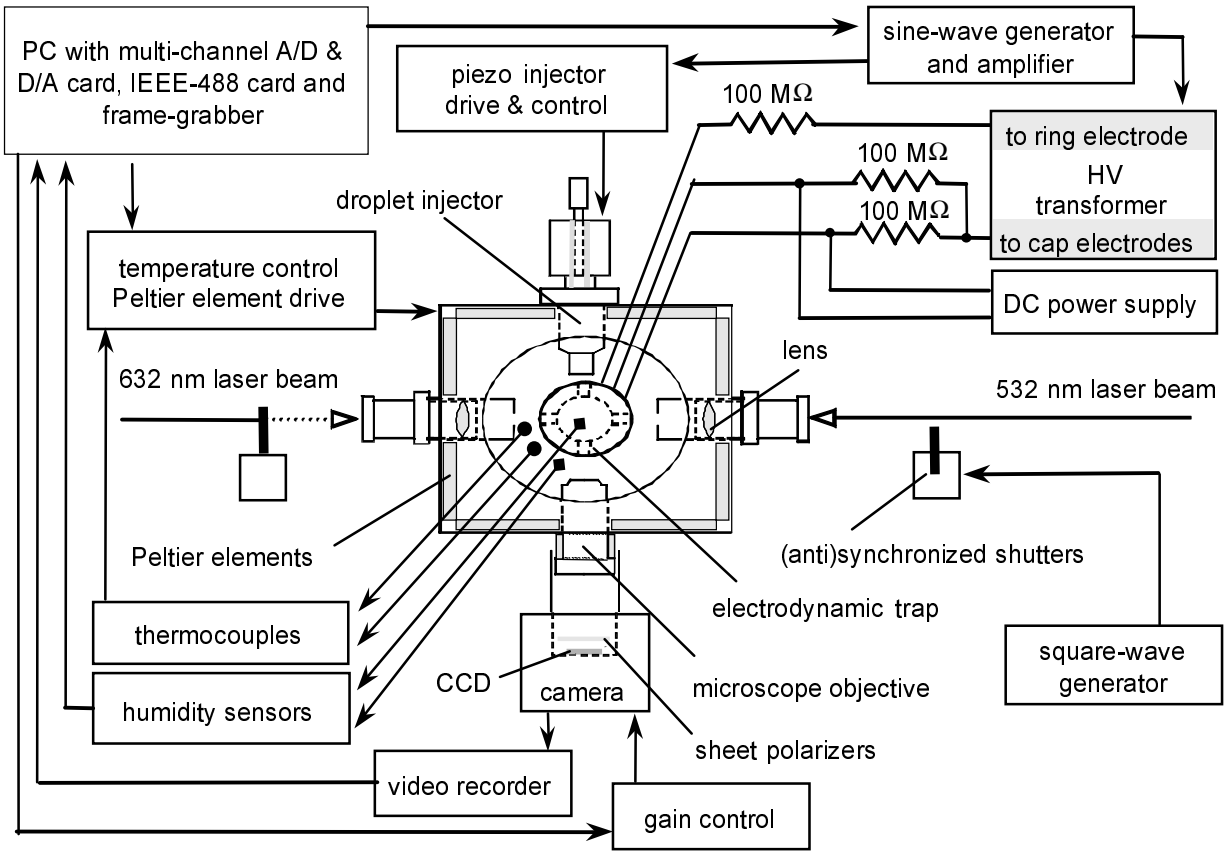

Figure 1. Experimental setup.

There was no gas flow through the chamber during the measurement of droplet evolution (see section 2.4).

2.3. The electrodynamic levitator and droplet injection

The electrodes of the trap are nearly hyperboloidal. The rotational symmetry, but not the exact shape, is crucial for stable trapping and precise measurements of particles that we encounter (micrometers' size liquid droplets). The caps are painted with black insulating enamel to suppress electric discharges due to the humid environment as well as to reduce stray light scattering. The middle ring electrode is painted with graphite in order to both reduce stray light scattering and suppress uneven charge accumulation (from charged droplets falling on the ring) which in turn prevents trapping field distortion. The AC (sine) driving voltage applied between the caps and the ring is supplied via 100 MΩ resistors. Usually we use ∼3000 V RMS at ∼310 Hz. Apart from that we could apply a DC voltage between the caps. It enabled us to move the particle along the vertical axis in order to find the sign of the charge of the droplet. Driving electrodes via high value resistors is the essential technical detail that enabled us to obtain stable trapping in humid environment by inhibiting electrical discharges.

There are four 2 mm's ports in the ring electrode for laser beams, droplet injection and observation.

We used a piezo type droplet injector (compare e.g.: [15]) driven from a pulse type transformer. The piezo tube is glued onto a glass tube which contains a liquid of interest. A Plexiglas rod was inserted coaxially into the glass tube in order to reduce the amount of liquid needed for the experiment. The nozzle was made of a 3 mm's thick Plexiglas or polysilane disk in the form of a cup inserted onto the end of the glass tube. First a conical hollow is lathed in it leaving a wall ∼0.5 mm thick at the tip of the cone. Then a circular hole of 0.1 mm's diameter is drilled.

The injection timing is controlled with a digital delay circuit utilizing the trap driving AC signal zero crossing as the reference. By choosing the proper injection phase we could control the sign and to a certain extent also the value of the charge deposited on the injected droplet.

2.4. The climatic chamber

The trap from the top and the droplet injector from the side are inserted into the ports of a small, double-walled, air tight chamber which can be cooled/heated with water cooled Peltier elements. There are two separately powered sections: upper and lower. Temperature inside the chamber is measured with two T-type thermocouples: one just above and one just below the trap. The above system enables us to get rid of vertical temperature gradients. Horizontal gradients were measured to be negligible. The chamber can be cooled below the dew point in ∼30 s' time and down to ∼240 K in several minutes.

The bottom and top chamber ports were used to control the humidity inside the chamber. There were two relative humidity sensors (HIH3610-2, Honeywell): one at each of these ports. First, the chamber was flushed with dry nitrogen in order to get rid of liquid water that accumulates in the chamber during the experiment via condensation and injection. Liquid water that accumulates on the trap causes severe distortions to the trapping field and deteriorates the trapping ability. Next, a filtered humid air (obtained by bubbling through distilled water) was flowed through the chamber from the bottom to the top port. When the required S and satisfactory S gradient were reached, the flow was stopped to enable uninfluenced trapping. Between the instants of trapping the chamber was flushed with humid air to maintain required humidity conditions, since otherwise, especially for high S, water vapor condenses inside the chamber due to the presence of the ports and S falls in time.

2.5. Optical data acquisition system and data processing

Two counterpropagating laser beams were used: He-Ne 632 nm (red light), ∼ 18 mW CW and Nd:YAG 532 nm (green light), ∼ 25 mW CW (power measured in front of the lasers). There were two antisynchronized shutters, one in each beam path, driven at ∼10 Hz. The laser beams were s polarized (i.e. perpendicularly to the scattering

plane), vertically in our case. The light scattered by the trapped particle was collected through the port in the ring electrode with a microscope objective positioned in the scattering plane at right angle to the direction of the incident beams. The numerical aperture of the system was ~ 0.17. Behind the objective, just in front of the CCD chip there were two sheet polarizers with polarization directions set perpendicularly dividing the field of view in two. This enables us to record scattering images on s and sp (crossed) polarizations simultaneously. The images are collected with a B/W CCD (K15, Philips) camera with gain controlled manually. The images are digitized with an 8-bit frame-grabber for further processing.

Mie scattering patterns recorded during the experiment (for details see: [8, 14]) represent the scattered light intensity I on s and ps (depolarization) polarizations as a function of angles: θ (azimuth in the observation plane) and ϕ (elevation) (see e.g. [16, 17]). We determined radius a of a droplet and its refractive index by direct fitting of Mie theory to experimental $I(\theta)$ for the s polarization of the scattered light. This method enables the access to the imaginary part of the effective refractive index (compare averaging method [8]) which is necessary in case of inclusions exhibiting non-negligible absorption.

2.6. AFM measurement

The AFM was operated in tapping mode and the tip curvature radius was ~ 20 nm. We used two types of samples for the AFM measurement. A drop of about 3 μl of fullerene suspension, prepared as described in section 2.2, was: (i) air-dried or (ii) spin-coated on the cover glass (No.1, Marienfeld). The local surface roughness of the cover glass was found to be below 1nm.

In case of the air dried sample, all the fullerene material remained on the glass. Then we were able to find the average fullerene layer thickness with AFM measurement and estimate the initial fullerene mass concentration to be $\sim 3\mu$g/ml. Aggregates of (average) radius from ~ 8 nm to ~ 500 nm (see figure 2) were found in these samples. The aggregates size distribution was of a power-law type. This is in agreement with the TEM measurements described in [11], where the authors concluded that in case of such size distribution, the aggregation must have been diffusion limited and must have lead to fractal clusters.

In the spin-coated sample a fine crystallite fraction dominated (see figure 3). Purely mechanical method of suspension preparation (pulverization and washing by low power sonication) seems to favor coarse and very fine fraction. Coarse fraction gets filtered out. Since most of the suspension drop leaves the cover glass while spin-coating, there is also no time for secondary aggregation into a coarse fraction.

The comparison of figures 2 and 3 indicates that it is aggregation, due to water evaporation, from fine crystallites, that is responsible for microscopic properties of suspension droplet at the later stages of the droplet evolution. We estimated the diameter of the elementary building block to be ~ 8 nm.

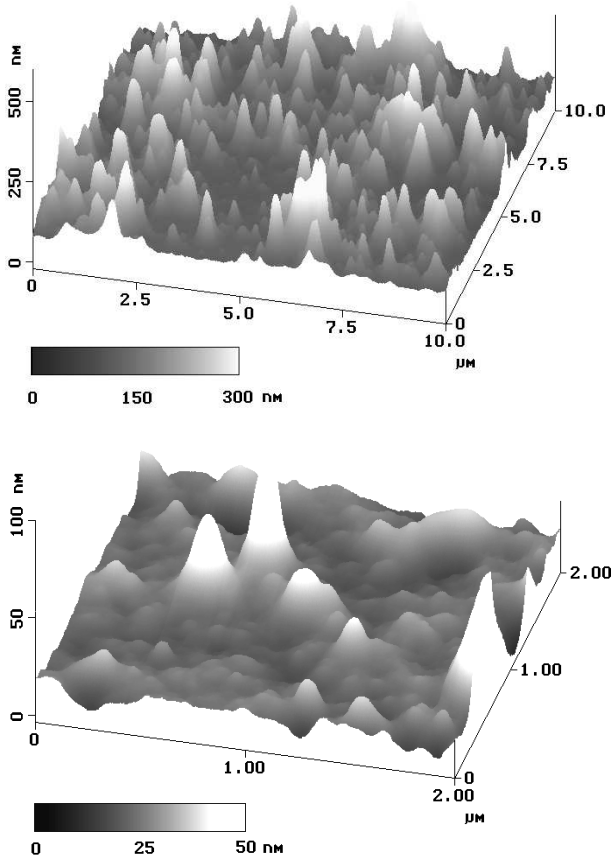

Figure 2. AFM images (3D representation, two magnifications) of a sample obtained by air drying of the water fullerene suspension.

3. Discussion

3.1. General results

The experiment yielded a variety of $\varepsilon_{eff}(R)$ evolution scenarios even for seemingly identical conditions. It may indicate that the initial stage of the evolution of the suspension droplet, which takes place between the emerging of the droplet from the nozzle and its arrival at the trap center, was quite random. In figure 5 we present two quite different $\varepsilon_{eff}(R)$ evolution scenarios corresponding to $R(t)$ evolutions presented in figure 4. Figures 4 (a) and 5 (a) correspond most probably to a particle with high fullerene content, nearly dry in the end, while figures 4 (b) and 5 (b) correspond to a particle of rather low fullerene content. The wet-dry transition was not so obvious for fullerene suspensions as for SiO_2 and PS spheres suspension [8] since Mie scattering patterns persisted (though a little speckled) all the time, not giving way to "bulk speckle". This could be caused by high deliquescence of particle as well as by absence of structures large enough (polycrystalline particle). It is well known [18] that it is difficult to get rid of residual solvent from fullerenes. For water it requires the temperature over $\sim$ 430 K which we can not achieve in our climatic chamber. Though we lowered the

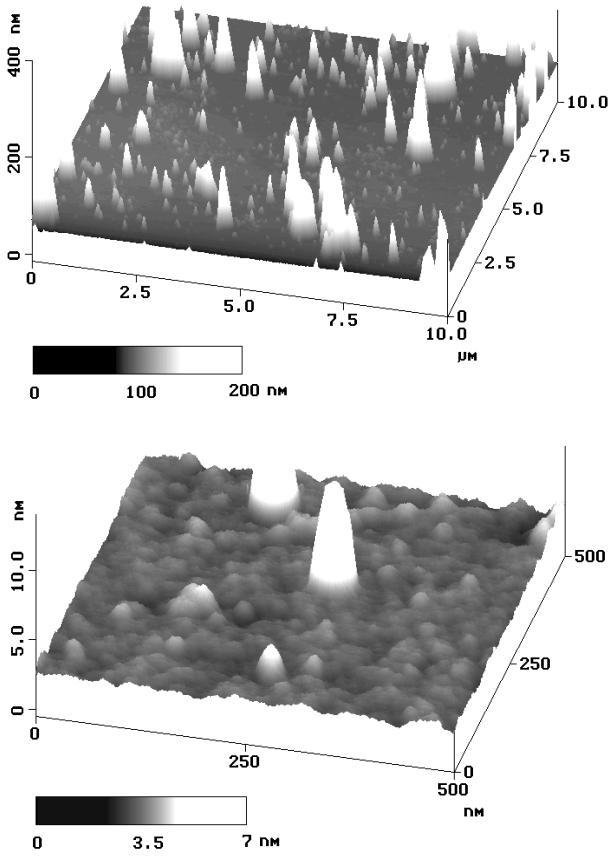

Figure 3. AFM images (3D representation, two magnifications) of a sample obtained by spin coating of the water fullerene suspension.

relative humidity in the chamber below 3% we did not observe the transition to "bulk speckle". On the other hand, since our AFM observations as well as TEM observations [11] revealed a wide spectrum of fullerene nanocrystallite sizes in suspension, we would expect very few voids in the totally dry polycrystalline particle. For such a dry particle the value of the real part of refractive index n should approach that of the bulk material ($\sim$ 2 for 632 nm and $\sim$ 2.1 for 532 nm [19]). For fullerene nanocrystallites suspension we might expect small but non-negligible imaginary part of refractive index (absorption) when the packing becomes dense (compare [19]). However, the effect was hardly perceivable. For some composite particles the imaginary part of refractive index gradually appeared well after the stabilization of particle (droplet) size. For other particles there was no imaginary part of the refractive index even after the stabilization. We would thus consider particles with non-negligible imaginary part of refractive index as dry. This would also indicate that particles may stabilize as wet. In this work we dealt only with wet particles with purely real refractive index. This corresponds to the region left of the vertical dashed lines in figures 4 (a) and (b). We shall discuss the issue of the imaginary part of refractive index of fullerene water suspension in a separate paper.

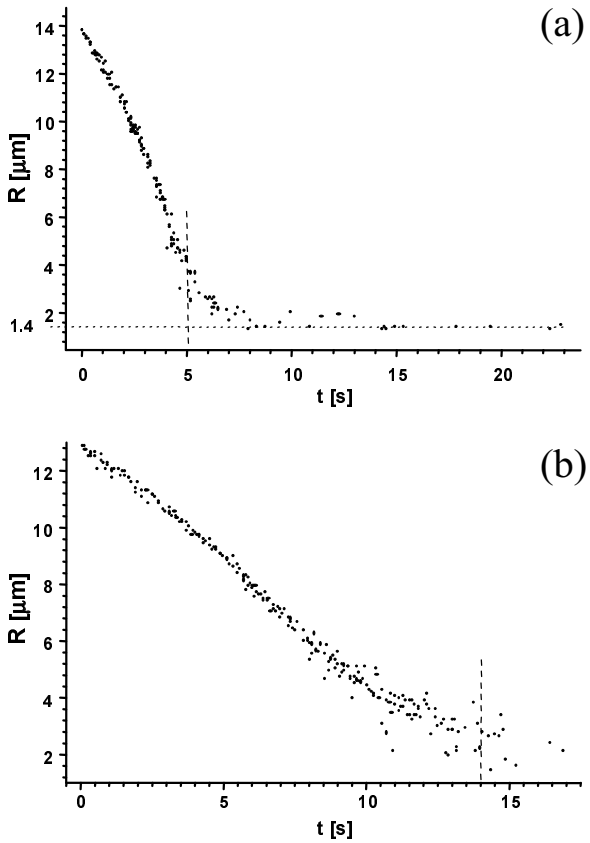

Figure 4. Evolution of the composite droplet radius for: (a) high fullerene contents, $T = 294.9$ K, $S = 95$ %, $p_{atm} = 979$ hPa and (b) low fullerene contents, $T = 296.3$ K, $S = 98$ %, $p_{atm} = 1006$ hPa. The region of our interest (wet particle) was to the left of the vertical dashed lines.

Suspension of fullerene nanocrystallites in water is more complicated than monodispersive nanosphere suspensions previously studied by us [8]. The aggregation and percolation of solid phase is not suppressed and the inclusions may be highly polydyspersive. Thus we could encounter two kinds of resonances: (i) associated with fullerene structures size (not necessarily spherical) and (ii) associated with the average distance between neighboring fullerene structures. As the droplet shrinks due to the evaporation, the size of fullerene structures grows, while the distance between them diminishes. Since the light scattering experiment was conducted for 2 wavelengths simultaneously, we should be able to distinguish the type of resonance by its relative position for green and red light versus the droplet radius. Indeed, in both figures the resonance for red light is shifted to the right in comparison to the same for green. And this behavior could be found in all our observations. Thus we infer that we encountered resonances of type (ii) associated with the diminishing of the average distance between neighboring fullerene structures. This would indicate that the aggregates usually do not grow to the size enabling resonant behavior, which we would expect near half the light wavelength $\lambda/2$.

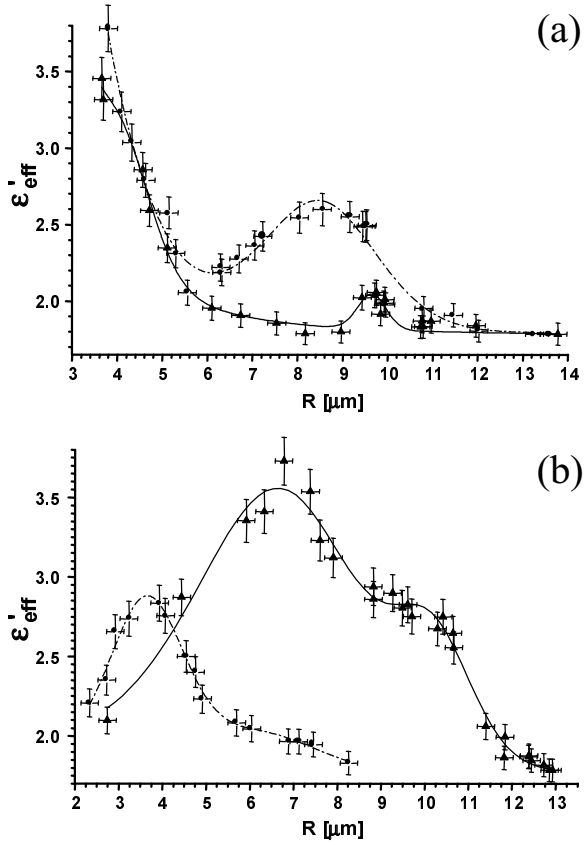

Figure 5. The real part of effective dielectric function of the composite droplet as a function of droplet radius, corresponding to figure 4: circles and dash-dot line - green light and triangles and solid line - red light.

3.2. Effective dielectric function

In order to further interpret our experimental results, we inevitably must deal with mid-range filling factors and eventually also with structures of the order of the wavelength, where practically no effective medium theory holds. For the sake of simplicity, we start with the Maxwell-Garnet mixing rule, which holds for very low and very high (inverted composition - water inclusions in fullerene material) filling factors. Then we correct it in a phenomenological way for mid-range filling factors. We have extended the model previously proposed for description of water droplets with well defined spherical inclusions [8].

The Lorentz local field consists of the light electric field inside water droplet E_{Mie}, described by Mie theory, and the field ΔE created by polarization charges on the "Lorentz sphere" [20]:

$$E_{local} = E_{Mie} + \Delta E \ , \tag{1}$$

where

$$\Delta E = \frac{P}{3\varepsilon_0\varepsilon_m} = \frac{1}{3\varepsilon_0\varepsilon_m} E_{local} \sum n_j\alpha_j = \varepsilon_0(\varepsilon_{eff} - \varepsilon_m)E_{Mie} \ , \tag{2}$$

n_j and α_j are the number density and polarizability of the j-th particle species, ε_m is the dielectric function of the medium (water), P is polarization. Therefore

$$\frac{E_{Mie}}{E_{local}} = 1 - \frac{\sum n_j\alpha_j}{3\varepsilon_0\varepsilon_m} \text{ and } \varepsilon_{eff} = \varepsilon_m + \frac{\sum n_j\alpha_j}{\varepsilon_0}\ \frac{E_{local}}{E_{Mie}}\ . \tag{3}$$

In the end this leads to Loretz-Lorenz formula:

$$\varepsilon_{eff} = \varepsilon_m \frac{1 + \frac{2}{3\ \varepsilon_0\varepsilon_m}\sum n_j\alpha_j}{1 - \frac{1}{3\ \varepsilon_0\varepsilon_m}\sum n_j\alpha_j}\ . \tag{4}$$

For a drop (of water) of radius R containing inclusions of the total volume V_{dry}

$$\varepsilon_{eff} = \varepsilon_m \frac{1 + \frac{2f}{3\ \varepsilon_0\varepsilon_m}\frac{\sum N_j\alpha_j}{V_{dry}}}{1 - \frac{f}{3\ \varepsilon_0\varepsilon_m}\frac{\sum N_j\alpha_j}{V_{dry}}}\ , \tag{5}$$

with filing factor $f = \frac{3V_{dry}}{4\pi R^3}$ and N_j being the number of j-th inclusion particles.

3.3. Polarizability

For inclusions of dielectric function ε_f, essentially smaller than λ, uniformly distributed in a medium (water) the total polarizability $\sum n_j\alpha_j$ can be expressed (after Wiener) as:

$$\sum_j n_j\alpha_j = f\frac{\varepsilon_f - \varepsilon_m}{\varepsilon_f + 2\varepsilon_m} \cdot 3\ \varepsilon_0\varepsilon_m \tag{6}$$

A composite medium consisting of species forming a broad variety of topological structures (like fractals, in our case fullerene crystallites), can be perceived as composed of resonance cavities tuned better or worse to light wavelength. To some extent it is equivalent to describing such a material with a set of harmonic oscillators (compare: [16, 21]). The total polarizability has a form of the sum of resonance terms then:

$$\sum_j n_j\alpha_j = \sum_k \frac{A_k}{\omega_k^2 - \omega^2 - i\gamma_k\omega}\ , \tag{7}$$

where ω stands for light frequency, γ_k describes resonance width and A_k is a constant. Under ordinary conditions there exists a nonuniform distribution of characteristic frequencies ω_k. This leads to a gaussian profile of resonance instead of a lorentzian profile given by uniformly damped oscillator. We describe polarizability of a composite medium as of harmonic oscillators being nonuniformly broadened. This broadening arises from e.g. nonuniform spatial distribution of polarizability associated with the distribution of density of different species n_j. Interaction of light of varying wavelength with such a medium leads to manifestation of various resonances. Modifying the density of the composite medium should be quite equivalent. The nonuniformity of distribution of eigenfrequencies of the medium should lead to gaussian resonance profiles. We describe the total polarizability by the series of resonators, with naturally distributed resonance frequencies. Since the expression should necessarily hold for the limiting cases - a very small and a very large filling factor - we write:

$$\sum_j n_j\alpha_j = \frac{1}{R^3}\left\{A_0 + \sum_{k>1} A_k \exp\left[-\left(\frac{\omega - \omega_k}{\gamma_k}\right)^2\right]\right\}\ , \tag{8}$$

where:

$$A_0 = V_{dry}\frac{\varepsilon_f - \varepsilon_m}{\varepsilon_f + 2\varepsilon_m} \ . \tag{9}$$

The frequencies ω_k should correspond to characteristic sizes r_k of structures involved: $\omega_k \sim 1/r_k$. For resonances associated with average distance between neighboring inclusions, r_k should, in turn, be proportional to the droplet radius R: $\omega_k = C_k/R$, where C_k is a constant. Then

$$\frac{\omega - \omega_k}{\gamma_k} = \frac{\omega - \frac{C_k}{R}}{\gamma_k} \ , \tag{10}$$

where $\omega = 2\pi c/\lambda$. Finally, we can rewrite the expression 5 describing effective dielectric function of the drop with inclusion as follows:

$$\varepsilon_{eff} = \varepsilon_m \frac{1 + \frac{2M(R)}{R^3}}{1 - \frac{M(R)}{R^3}} \ , \tag{11}$$

where

$$M(R) = A_0 + \sum_{k>1} A_k \exp\left[- \left(\frac{\omega - \frac{C_k}{R}}{\gamma_k} \right)^2 \right] \ .$$

The factor M can be perceived as a modification of the local field arising from multipolar effects of scattering on inclusions [3, 22] (for higher filling factors these are rather water inclusions in fullerene medium), near field effects [23] (for distances between neighboring inclusions below 4-5 λ interaction can not be neglected), interference of fields multiply scattered along different paths (weak localization, for distances between scatterers of the order of λ has to be taken into consideration) [24], etc.

3.4. Further data interpretation

The experimental data in figures 5 (a) and (b) has been fitted with formula 11. We used the smallest reasonable value of k. One and two resonances were detected for in figures 5 (a) and (b) respectively. As we mentioned before, the comparison of red and green scattering allows us to attribute them to (diminishing) average distance between neighboring scatterers. Then we might try to infer about the size of scatterers (fullerene nanocrystallites) involved. The aggregation scenario, however, is not fully known. It is assumed to be diffusion limited [11, 25]. On the basis of our AFM study we can assume that at the middle stage of the evolution when the resonance is observed, there is a distribution of inclusion sizes in which finer fractions prevail. In case of the evolution leading to the dry or nearly dry particle, as in figure 4 (a), V_{dry}, corresponding to $R(t \to \infty)$, is known. We further assume that inclusions associated with the resonance make up e.g. $0.75V_{dry}$ and that the average distance between neighboring scatterers associated with the resonance is of the order of λ/n_w, where n_w is the real part of the refractive index of water. Then it is possible to find an approximate average radius of the scatterer in question in the form:

$$r_{incl} \simeq R(t \to \infty)\frac{\lambda}{2R_{res}n_w} \ , \tag{12}$$

where R_{res} is the radius of the composite droplet corresponding to the resonance.

For the evolution presented in figures 4 (a) and 5 (a) ($T = 294.9$ K), $R(t \to \infty) = 1.41$ μm, $R_{res}(red) = 9.64$ μm and $R_{res}(green) = 8.47$ μm, and $n_w(red) = 1.33209$ and $n_w(green) = 1.33551$. From equation 12 we ideally should obtain the same results for both wavelength. And indeed $r_{incl}(red) \simeq 35$ nm and $r_{incl}(green) \simeq 33$ nm which is fairly consistent as well as in agreement with the AFM observations (compare figures 2 and 3). Thus we can conclude that $r_{incl} \simeq 34$ nm.

4. Conclusions

Evaporation of water (hosting medium) from the droplet of suspension leads to the increase of the concentration of the inclusions. In such a case, the single wavelength scattering scans through eventual resonances associated with the microscopic properties of the suspension. The resonances associated with inclusions structure can be told from resonances associated with distances among inclusions by observing the relative positions of resonance peaks in two color measurement. For water suspensions of fullerenes investigated in this work, only resonances associated with distances among inclusions (possibly average distance between neighboring scatterers) were detected. Having applied a few reasonable assumptions we obtained the average radius of inclusions involved in the resonance to be ~ 34 nm. Our light scattering observations seem to be consistent with our AFM observations as well as Andrievsky TEM observations [11].

Acknowledgments

This work was supported by Polish State Committee for Scientific Research grant No. 2 P03B 102 22.

References

[1] Barth H G and Sun S-T 1993 Particle size analysis *Anal. Chem.* **65** 55R–66R

[2] Megens M, van Kats C M, Bösecke P and Vos W L 1997 *In situ* characterization of colloidal spheres by synchrotron small-angle X-ray scattering *Langmuir* **13** 6120–9

[3] Chýlek P, Ramaswamy V and Cheng R J 1984 Effect of graphitic carbon on the albedo of clouds *J. Atmos. Sci.* **41** 3076–84

[4] Ackerman A S, Toon O B, Stevens D E, Heymsfield A J, Ramanathan V and Velton E J 2000 Reduction of tropical cloudiness by soot *Science* **288** 1042

[5] Markel V A and George T F 2001 *Optics of Nanostructured Materials* (New York: Wiley) pp 335–466

[6] Markel V A and Shalaev V M 1999 Absorption of light by soot particles in micro-droplets of water *J. Quantitative Spectroscopy & Radiative Transfer* **63** 321–39

[7] Markel V A 2002 The effects of averaging on the enhancement factor for absorption of light by carbon paricles in microdroplets of water *J. Quantitative Spectroscopy & Radiative Transfer* **72** 765–74

[8] Jakubczyk D, Derkachov G, Zientara M, Kolwas M and Kolwas K 2004 Local-field resonance in light scattering by a single water droplet with spherical dielectric inclusions *J. Opt. Soc. Am. A* **21** 2320–2323

[9] Da Ros T and Prato M 1999 Medical chemistry with fullerenes and fullerene derivatives *Chem. Commun.* (issue 8) 663–9
[10] Scrivens W A, Tour J M, Creek K E and Pirisi L 1994 Synthesis of ^{14}C-labelled C_{60}, its suspension in water, and uptake by human karatinocytes *J. Am. Chem. Soc.* **116** 4517–8
[11] Andrievsky G V, Klochkov V K, Karyakina E L and Mchedlov-Petrossyan N O 1999 Studies of aqueous colloidal solutions of fullerene C_{60} by electron microscopy *Chem. Phys. Lett.* **300** 392–6
[12] Andrievsky G V, Kosevich M V, Vovk O M, Shelkovsky V S and Vashchenko L A 1995 On the production of an aqueous colloidal solution of fullerenes *J. Chem. Soc., Chem. Commun.* **12** 1281–2
[13] Paul W 1990 Electromagnetic traps for charged and neutral particles *Rev. Mod. Phys.* **62** 531–540
[14] Jakubczyk D, Zientara M, Derkachov G, Kolwas K and Kolwas M 2004 Investigation of the evolution of the charged water droplets in the electrodynamic trap *Tenth Joint Int. Symp. on Atmospheric and Ocean Optics/Atmospheric Physics. Part II: Laser Sensing and Atmospheric Physics; Proc. SPIE* **5397** 23–33
[15] Lee E R and Perl M L 1999 Universal Fluid Droplet Ejector *U.S. Pat. No. 5943075*
[16] Bohren C F and Huffman D R 1998 *Absorption and Scattering of Light by Small Particles* (New York: Wiley)
[17] Mishschenko M I, Hovenier J W and Travis L D 2000 *Light Scattering by Nonspherical Particles* (San Diego: Academic)
[18] Huffman D R 1991 Solid C_{60} *Physics Today* **44** 22–9
[19] Ren S L, Wang Y, Rao A M, McRae E, Holden J M, Hager T, Wang K, Lee W-T, Ni H F, Selegue J and Eklund P C 1991 Ellipsometric determination of the optical constants of C_{60} (Buckminsterfullerene) films *Appl. Phys. Let.* **59** 2678–80
[20] Kreibig U and Vollmer M 1995 *Optical Properties of Metal Clusters* (Berlin: Springer)
[21] Demtröder W 1988 *Laser Spectroscopy, Basic Concepts and Instrumentation* (Berlin: Springer)
[22] Stroud D and Pan F P 1978 Self-consistent approach to electromagnetic wave prop-agation in composite media: Application to model granular metals *Phys. Rev. B* **17** 1602–10
[23] Xu H 2003 A new method by extending Mie theory to calculate local field in outside/inside of aggregates of arbitrary spheres *Phys. Lett. A* **312** 411–9
[24] van Tiggelen B A, Lagendijk A, van Albada M P and Tip A 1992 Speed of light in random media *Phys. Rev. B* **45** 12233–43
[25] Bonczyk P A and Hall R J 1991 Fractal properties of Soot Agglomerates *Langmuir* **7** 1274–80